to the tetramer is $k_1/k_T \simeq 3$. This value is a lower limit, as the methylene resonance of the butyllithium remaining at the end of the reaction has a chemical shift identical with that of the monoalkoxy mixed aggregate. In the final state the butyllithium is apparently complexed to the alcoholate product. Although we once again refuse to speculate on the nature of this particular aggregate, we note that we observed it systematically whenever the alcoholate was present in a large excess relative to the butyllithium.

In experiments involving a greater proportion of the dialkoxy mixed aggregate, we find that it has approximately the same reactivity as the dimer relative to the tetramer $k_{DA}/k_T = 7 \pm 4$. The trialkoxy aggregates appeared in other experiments to be even more reactive, but a quantitative estimation proved to be impossible.

We feel that these results may have a direct bearing on the kinetic order of butyllithium in its reactions. Butyllithium which is in a mixed Li_4 aggregate with three alkoxide ligands, or in a mixed Li_2 aggregate with one alkoxide ligand, will behave *kinetically as a monomer*. Any reaction of butyllithium in THF at room temperature will occur in the presence of enolate ions, formed by the decomposition of the solvent. According to Holm's figures,[9] a solution originally 10^{-2} M in butyllithium will form 3 mM acetaldehyde enolate after 30 s at 25 °C. (In our experiments no decomposition was apparent during 1 h at −78 °C.) Adventitious oxygen will give rise to alkoxides. These impurities will lead to partial order kinetics. The significance of this effect will depend of course on the concentration of oxide ligands and also on the selectivity of the substrate toward different aggregates.

Conclusions

By use of the rapid injection NMR technique at temperatures between −80 and −90 °C we have shown the following: (a) The rate of the scission of hexameric butyllithium in THF into tetramer and dimer is twice that of the dissociation of tetramer into dimer. (b) Tetrameric butyllithium can react with benzaldehyde more rapidly than it dissociates into dimer. (c) Dimeric butyllithium is more reactive than the tetramer toward cyclopentadiene and benzaldehyde, and in the latter case the difference is by a factor of 10. (d) Increased substitution of alkyl ligands by alkoxy ligands in mixed Li_4 aggregates increases the reactivity of the remaining alkyl groups. (e) In the reaction of butyllithium with benzaldehyde, the product 1-phenylpentanolate is formed in a nonequilibrated, highly reactive state, which allows it to compete with tetrameric butyllithium as a nucleophile. Analogous effects on the reactivity and selectivity of other organometallic reagents are highly probable, and we are confident that the RINMR method will continue to provide insights into this apparently complex, but very important chemistry.

Acknowledgment. We thank Professors H. Dahn and P. v. R. Schleyer for helpful discussions, Professor D. Seebach for communication of results prior to publication, and the Swiss National Science Foundation for financial support.

Registry No. THF, 109-99-9; BuLi, 109-72-8; PhCHO, 100-52-7; cyclopentadiene, 542-92-7.

Kinetics and Mechanism of Self-Protonation Reactions in Organic Electrochemical Processes

Christian Amatore,[1b] Giulio Capobianco,[1a] Giuseppe Farnia,[1a] Giancarlo Sandonà,[1a] Jean-Michel Savéant,*[1b] Maria Gabriella Severin,[1a] and Elio Vianello*[1a]

Contribution from the Istituto di Chimica Fisica ed Elettrochimica, Università di Padova, 35131 Padova, Italy, and the Laboratoire d'Electrochimie de l'Université de Paris 7, 75221, Paris Cedex 05, France. *Received August 6, 1984*

Abstract: Anion radicals and dianions produced from the electrochemical reduction of organic molecules are basic species. In the case where the parent compound is a stronger acid than the acids present in the reaction medium, it may react with the basic species resulting from its reduction giving rise to a self-protonation electrochemical process. Determination of the reaction stoichiometry is a necessary first step in the assignment of the reaction mechanism. However, a detailed kinetic analysis is required for identifying the basic species which actually react with the parent molecule, assigning the rate-controlling steps, and determining the pertinent rate constants. This has been carried out on the examples of six molecules bearing acidic hydrogens: phthalimide, 1,3-diphenyl-2-methylindene, 4,5-methylenephenanthrene, and the three nitrophenol isomers, using linear sweep and cyclic voltammetry as well as conventional homogeneous kinetic techniques.

The electrochemical reduction of organic compounds is quite generally associated with the production of basic species in the general sense. Several types of bases and different modes of reactions with the acids present in the reaction medium may occur. A typical example is provided by the reduction of aromatic hydrocarbons or heterocycles leading to the formation of dihydrogenated products.[2]

The use of aprotic solvents such as dimethylformamide (DMF) allows the observation of two different hydrogenation pathways according to the relative strength of the proton donors (DH) present in the medium and of the basic species formed upon successive reduction of the starting molecule, i.e., the anion radical and the dianion.

In carefully dried media[2d] the two latter species are stable in the time scale of low sweep rate cyclic voltammetry, i.e., seconds, giving rise to two reversible waves corresponding to the successive formation of the anion radical and the dianion:

$$AH + e \rightleftarrows AH^{-\cdot}$$

$$AH^{-\cdot} + e \rightleftarrows AH^{2-}$$

In the presence of small amounts of water, the dianion is protonated whereas the less basic anion radical is not:

$$AH^{2-} + DH \rightarrow AH_2^- + D^-$$

(1) (a) Istituto di Chimica Fisica, Università di Padova. (b) Laboratoire d'Electrochimie, Université de Paris 7.

(2) (a) Baizer, M. M. "Organic Electrochemistry"; Marcel Dekker: New York, 1973. (b) Peover, M. E. "Electroanalytical Chemistry"; Bard, A. J., Ed.; Marcel Dekker: New York, 1970; Vol. 2, pp 1–51. (c) Perichon, J. "Encyclopedia of Electrochemistry of the Elements"; Bard, A. J., Lund, H., Eds.; Marcel Dekker: New York, 1978; Vol. XI, pp 71–161. (d) Jensen, B. S.; Parker, V. D. *J. Am. Chem. Soc.* **1975**, *97*, 5211–5217. (e) Dietz, R.; Peover, M. E. *Trans. Faraday Soc.* **1966**, *62*, 3535–3542. (f) Dietz, R.; Larcombe, B. E. *J. Chem. Soc. B* **1970**, 1369–1373. (g) Amatore, C.; Gareil, M.; Saveant, J. M. *J. Electroanal. Chem.* **1983**, *147*, 1–38.

0002-7863/85/1507-1815$01.50/0

$$AH_2^- + DH \rightarrow AH_3 + D^-$$

as revealed by the fact that the second wave becomes irreversible whereas the first remains reversible. It is noteworthy that the monoanion AH_2^- appears as a stronger Brønsted base than the anion radical $A^{-\cdot}$.[2e,f] Addition of a stronger proton donor, such as phenol, renders the first wave irreversible and increases its height up to two electrons per molecule revealing the protonation of the anion radical[2g] (scheme A).

$$AH + e \rightleftarrows AH^{-\cdot}$$

$$AH^{-\cdot} + DH \rightleftarrows AH_2^{\cdot} + D^-$$

$$AH_2^{\cdot} + e \rightleftarrows AH_2^- \text{ and/or } AH_2^{\cdot} + AH^{-\cdot} \rightarrow AH_2^- + AH \qquad (A)$$

$$AH_2^- + DH \rightarrow AH_3 + D^-$$

$$AH + 2e + 2DH \rightarrow AH_3 + 2D^-$$

Different electron-transfer produced bases interfere in the cases where the starting molecule contains a nucleofugic group.[2a,3] The anion radical may then cleave before abstracting a proton from the medium[4] (scheme B). Here proton abstraction involves the

$$AX + e \rightleftarrows AX^{-\cdot}$$

$$AX^{-\cdot} \rightarrow A^{\cdot} + X^-$$

$$A^{\cdot} + e \rightleftarrows A^- \text{ and/or } A^{\cdot} + AX^{-\cdot} \rightarrow A^- + AX \qquad (B)$$

$$A^- + DH \rightarrow AH + D^-$$

$$AX + 2e + DH \rightarrow AH + X^- + D^-$$

anion A^-. As in the preceding case the overall stoichiometry involves two electrons per molecule. In this connection it is important, for the discussion below, to note that the second electron may be transferred concurrently from the electrode or from the anion radical in the solution.[2g,3b,c] The first pathway is commonly referred to as an ECE (electrochemical–chemical–electrochemical) mechanism and the second to as a DISP mechanism (disproportionation of two species having formally the same oxidation degree).[5]

It should also be emphasized that the electron-transfer-produced anions may react with acids other than protons. Electrophiles such as alkyl halides and carbon dioxide can play this role.[6]

The above discussion implicitely assumed that the starting molecule, AH or AX, is a weaker Brønsted or Lewis acid than the acids present in the medium. If not the case, an interesting situation arises where the starting compound serves as an acid neutralizing the bases produced upon its one- or two-electron reduction.

Several examples of such processes involving either two-electron or one-electron generated bases have been reported. Reactions of the first type can be found in the electrochemistry of compounds bearing at least one hydrogen atom and nucleofugic moiety as a quaternary ammonium, phosphonium, tertiary sulfonium, ether, thioether, sulfonamide, or sulfone group.[7] The reduction of PPh_4^+ in DMF illustrates the case where the reaction between the two-electron-generated base and the starting molecule is a Lewis acid–base reaction rather than a proton transfer.[7f]

The reduction of several organic compounds in aprotic solvents has been interpreted as belonging to the second category, i.e., as involving proton transfer between the initial anion radical and the starting molecule. This is the case of phthalimide,[8a,b,9a] uracil,[8c] hydroxypyrimidine,[8d] thymine,[8e] uridine,[8f] 4-aminopyrimidine,[8g] isatin,[9b] nitrophenols,[9c,d] phenyl-substituted indenes,[9e] 2,2-dimethyl-5-nitroimidazole,[9f] 4,5-methylenephenanthrene,[10] and 9-substituted fluorenes.[11] The "father–son"[8h,12] (starting molecule–anion radical) step is followed by a further one-electron reduction of the protonated anion radical, yielding the corresponding anion which is itself protonated by the starting molecule. A possible mechanism is given in Mechanism I.

Mechanism I

$$AH + e \rightleftarrows AH^{-\cdot} \quad (0)$$

$$AH^{-\cdot} + AH \underset{k_{-1}}{\overset{k_1}{\rightleftarrows}} AH_2^{\cdot} + A^- \quad (1)$$

$$AH_2^{\cdot} + e \rightleftarrows AH_2^- \quad (2) \text{ and/or } AH_2^{\cdot} + AH^{-\cdot} \xrightarrow{k_2} AH_2^- + AH \qquad (2')$$

$$AH_2^- + AH \rightarrow AH_3 + A^- \quad (3)$$

$$AH + (2/3)e \rightarrow (2/3)A^- + (1/3)AH_3$$

The overall stoichiometry thus involves the exchange of 2/3 electron per molecule, conversion of 1/3 of the starting compound into the dihydrogenated product, and 2/3 into its conjugated base. Precise assignement of these stoichiometric factors is of essential importance to distinguish the above-described mechanism from another possible mechanism involving evolution of hydrogen:

$$AH + e \rightleftarrows AH^{-\cdot}$$

$$AH^{-\cdot} \rightarrow A^- + (1/2)H_2$$

$$AH + e \rightarrow A^- + (1/2)H_2$$

(3) (a) Hawley, M. D. "Encyclopedia of Electrochemistry of the Elements"; Bard, A. J., Lund, H., Eds.; Marcel Dekker: New York, 1980; Vol. XIV, pp 179–262. (b) Saveant, J. M.; Thiebault, A. *J. Electroanal. Chem.* **1978**, *89*, 335–346. (c) Amatore, C.; Chaussard, J.; Pinson, J.; Saveant, J. M.; Thiebault, A. *J. Am. Chem. Soc.* **1979**, *101*, 6012–6020.

(4) In the case of aliphatic compounds, particularly alkyl halides, the cleavage is so fast that the very existence of the anion radical as an actual intermediate between electron transfer and cleavage may be questioned: Eberson, L. *Acta Chem. Scand., Ser. B* **1982**, *36*, 533–543.

(5) (a) In good H-atom donor solvents which is the case of most aprotic organic solvents, the reduction of A· may also occur through H-atom abstractions:[5b,c]

$$A^{\cdot} + SH \rightarrow S^{\cdot} + AH$$

The solvent radical S· then undergoes, in the case, e.g., of acetonitrile and dimethyl sulfoxide, a further electron transfer reduction:

$$S^{\cdot} + e \rightleftarrows S^- \text{ and/or } S^{\cdot} + AX^{-\cdot} \rightarrow S^- + AX$$

which produces a base, S^-, which then abstracts a proton from the proton donor:

$$S^- + DH \rightarrow SH + D^-$$

(b) M'Halla, F.; Pinson, J.; Saveant, J. M. *J. Electroanal. Chem.* **1978**, *89*, 347–361. (c) M'Halla, F.; Pinson, J.; Saveant, J. M. *J. Am. Chem. Soc.* **1978**, *100*, 1506–1510.

(6) Lund, H.; Simonet, J. *J. Electroanal. Chem.* **1975**, *65*, 205–218.

(7) (a) Saveant, J. M. *Bull. Soc. Chim. Fr.* **1967**, 481–86. (b) Saveant, J. M.; Veillard-Royer, H. *Ibid.* **1967**, 2415–22. (c) Andrieux, C. P.; Saveant, J. M. *Ibid.* **1972**, 3281–3290. (d) Saveant, J. M.; Su, K. B. *Ibid.* **1972**, 3549–3556. (e) Saveant, J. M.; Su, K. B. *Electrochim. Acta* **1975**, *20*, 21–26. (f) Saveant, J. M.; Su, K. B. *J. Org. Chem.* **1977**, *42*, 1242–1248. (g) Cottrell, P. T.; Mann, C. K. *J. Am. Chem. Soc.* **1971**, *93*, 3579. (h) Gambino, S.; Martigny, P.; Mousset, G.; Simonet, J. *J. Electroanal. Chem.* **1978**, *90*, 105.

(8) (a) Leedy, D. W.; Muck, D. L. *J. Am. Chem. Soc.* **1971**, *93*, 4264–4270. (b) Cummings, T. E.; Elving, P. J. *Ibid.* **1978**, *94*, 123–145. (d) Wasa, T.; Elving, P. J. *Ibid.* **1978**, *91*, 249–264. (e) Cummings, T. E.; Elving, P. J. *Ibid.* **1979**, *102*, 237–248. (f) Bresnahan, W. T.; Cummings, T. E.; Elving, P. J. *Electrochim. Acta* **1981**, *26*, 691–697. (g) Wasa, T.; Elving, P. J. *J. Electroanal. Chem.* **1982**, *142*, 243–261. (h) Elving, P. J. *Can. J. Chem.* **1977**, *55*, 3392–3412.

(9) (a) Farnia, G.; Romanin, A.; Capobianco, G.; Torzo, F. *J. Electroanal. Chem.* **1971**, *33*, 31–44. (b) Farnia, G.; Capobianco, G.; Romanin, A. *Ibid.* **1973**, *45*, 397–404. (c) Farnia, G.; Mengoli, G.; Vianello, E. *Ibid.* **1974**, *50*, 73–89. (d) Farnia, G.; Roque da Silva, A.; Vianello, E. *Ibid.* **1974**, *57*, 191–202. (e) Dal Moro, A.; Farnia, G.; Marcuzzi, F.; Melloni, G. *Nouv. J. Chim.* **1980**, *4*, 3–5. (f) Roffia, S.; Gottardi, G.; Vianello, E. *J. Electroanal. Chem.* **1982**, *142*, 263–275.

(10) Janata, J.; Gendell, J.; Lawton, R. G.; Mark, H. B. *J. Am. Chem. Soc.* **1968**, *90*, 5226–5232.

(11) Nuntnarumit, C.; Hawley, M. D. *J. Electroanal. Chem.* **1982**, *133*, 57–72.

(12) According to this picturesque nomenclature, the above-described reactions involving the neutralization of the two-electron generated bases and the starting molecule should be termed "grandfather/grandson" reactions. This representation also points to the fact that the latter reaction are likely to be thermodynamically favored, while the "father–son" processes are up-hill reactions. It will indeed be seen in the following that "father–son" reactions are rather slow in most cases, allowing the kinetic analysis of the reaction mechanism to be carried out while "grandfather/grandson" reactions are extremely rapid, leading to voltammetric waves that are irreversible at any accessible sweep rate.

as hypothetized to occur in the reduction of nitrobenzyl derivatives,[13a] *p*-nitrobenzenesulfonamides,[13b,c] fluorenes and *p*-cyanoaniline,[13d] nitroaniline,[13e] and nitroimidazoles.[13f,g]

In the above-mentioned investigations neither kinetically based mechanism analysis nor rate constant determination has been reported. It was the purpose of the kinetic study described hereafter to fill this gap.

In the cases where the stoichiometry clearly rules out the hydrogen evolution mechanism, several important mechanistic questions arise which can be answered only on kinetic grounds.

(i) Is the anion radical actually involved as a basic agent in the abstraction of a proton from the starting molecule? Besides mechanism I, it is indeed conceivable that the dianion produced through a prior disproportionation step is the actual deprotonation agent leading to the same stoichiometry as mechanism I (see Mechanism II).

Mechanism II

$$AH + e \rightleftarrows AH^{-}\cdot$$

$$2AH^{-}\cdot \rightleftarrows A + AH^{2-}$$

$$AH^{2-} + AH \rightarrow AH_2^{-} + A^{-}$$

$$AH_2^{-} + AH \rightarrow AH_3 + A^{-}$$

$$\overline{AH + (2/3)e \rightarrow (2/3)A^{-} + (1/3)AH_3}$$

(ii) In the case where mechanism I does operate, is the second electron transfer occurring at the electrode (reaction 2, ECE pathway) or in the solution with $AH^{-}\cdot$ as the electron source (reaction 2′ DISP pathway)? This is an essential point to be addressed to understand which step governs the overall kinetics. In the case where the DISP pathway predominates, it is indeed conceivable that the rate-determining step is either the protonation step itself or the followup solution electron transfer, protonation acting as a preequilibrium. Mixed kinetic control by these two steps should also be investigated. The answer to these questions is required in order to derive meaningful rate constants as a starting point to relate the observed reactivity to the structure of the starting molecule.

It appears that the kinetics corresponding to mechanism I are formally the same as for the "DIM2" electrodimerization mechanism involving the coupling of the anion radical with the starting molecule followed by heterogeneous (ECE) or homogeneous (DISP) one-electron transfer to the resulting dimeric anion radical

$$A + e \rightleftarrows A^{-}\cdot \quad (0)$$

$$A^{-}\cdot + A \rightleftarrows {}^{-}A\text{-}A\cdot \quad (1)$$

$${}^{-}A\text{-}A\cdot + e \rightleftarrows {}^{-}A\text{-}A^{-} \quad (2)$$

and/or

$${}^{-}A\text{-}A\cdot + A^{-}\cdot \rightarrow {}^{-}AA\text{-}A^{-} + A \quad (2')$$

for which a formal kinetic treatment already exists.[14] There is no reaction 3 in this case which leads to a 1e instead of a (2/3)e stoichiometry. The kinetics are, however, the same since the rate-determining step precedes reaction 3.

The kinetic study of self-protonation has been carried out on two series of compounds. In the first, involving phthalimide, 1,3-diphenyl-2-methylindene, and 4,5-methylenephenanthrene, the reduction yields a 2e + 2H$^+$ product; in the second, involving nitrophenols, the reduction gives rise to the corresponding hydroxy phenylhydroxylamine (4e + 4H$^+$) for the 1 and 3 isomers and to the hydroxyamine (6e + 6H$^+$) for the 4 isomer. Besides coulometry and analysis of products, we used linear sweep and cyclic voltammetry to investigate the reaction mechanism with the exception of 4,5-methylenephenanthrene where the reaction was so slow that the conventional techniques of homogeneous kinetics could be used, following the decay of the anion radical, $AH^{-}\cdot$, by amperometry.

Table I. Kinetic Analysis of Self-Protonation Mechanisms by Linear Sweep Voltammetry: Pure Kinetic Control

kinetic regime	expression of the peak potential as a function of rate constants, sweep rate, and concentration
ECE_{irr}	$E_p = E^\circ = -0.05(RT/F) + RT/2F \ln (RTk_1C^\circ/Fv)$
ECE_{rev}	$E_p - E^\circ = -0.61(RT/F) + RT/2F \ln (k_1^2/k_{-1})(RTC^\circ/Fv)$
DISP1	$E_p - E^\circ = -0.40(R/F) + RT/2F \ln (RTk_1C^\circ/Fv)$
DISP2	$E_p - E^\circ = -0.64(RT/F) + RT/3F \ln (k_2k_1/k_{-1})(RTC^\circ/Fv)$

	variations of peak potential with sweep rate and concentration and peak width at 25 °C		
	$\partial E_p/\partial \log v$ (mV)	$\partial E_p/\partial \log C^0$ (mV)	$E_{p/2} - E_p$ (mV)
ECE_{irr}	29.6	29.6	58.3
ECE_{rev}	29.6	29.6	87.1
DISP1	29.6	29.6	58.3
DISP2	19.7	19.7	58.0

	competition parameters		
ECE_{rev}–ECE_{irr}	k_1/k_{-1}	$\rightarrow 0$	ECE_{rev}
		$\rightarrow \infty$	ECE_{irr}
ECE_{irr}–DISP1	$(k_2/k_1^{3/2})(Fv/RTC^\circ)^{1/2}$	$\rightarrow 0$	ECE_{irr}
		$\rightarrow \infty$	DISP1
DISP1–DISP2	$(k_{-1},k_1^{1/2}/k_2)(RTC^\circ/Fv)^{1/2}$	$\rightarrow 0$	DISP1
		$\rightarrow \infty$	DISP2
DISP2–ECE_{rev}	$(k_1^2/k_{-1}^{1/2}k_1)\cdot(RTC^\circ/Fv)^{1/2}$	$\rightarrow 0$	DISP2
		$\rightarrow \infty$	ECE_{rev}

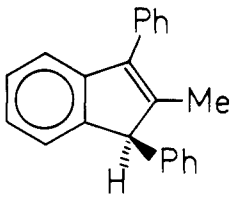

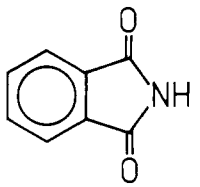

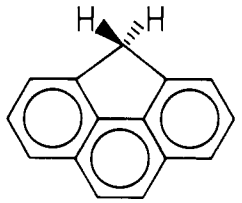

Results and Discussion

Procedures for the Kinetic Analysis of the Reaction Mechanism in Linear Sweep and Cyclic Voltammetry. As in any electrochemical kinetic problem involving the coupling of diffusion processes with homogeneous reactions,[2g,15] we can distinguish two main kinetic regimes.[16]

(13) (a) Bartak, D. E.; Hawley, M. D. *J. Am. Chem. Soc.* **1972**, *94*, 640–642. (b) Asirvatham, M. R.; Hawley, M. D. *J. Electroanal. Chem.* **1974**, *53*, 293–305. (c) Santelices, C.; Hawley, M. D. *Ibid.* **1977**, *84*, 387–397. (d) Borhani, K. J.; Hawley, M. D. *Ibid.* **1979**, *101*, 407–417. (e) Mairanovskii, S. G.; Sosonkin, I. M.; Ponomareva, T. K. *Elektrokhimiya* **1978**, *14*, 567–570 (*Engl. Trans.* 479–482). (f) Lopyrev, V. A.; Larina, L. I.; Rakhmatulina, T. N.; Shibanova, E. F.; Vakul'skaya, T. J.; Voronkov, M. G. *Dokl. Akad. Nauk SSSR* **1978**, *242*, 142–145 (*Engl. Trans.* 770–73). (g) Vakul'skaya, T. I.; Larina, L. I.; Nefedova, O. B.; Petukhov, L. P.; Voronkov, M. G.; Lopyrev, V. A. *Khim. Geterotsikl. Soedin.* **1979**, *10*, 1398–1403 (*Engl. Trans.* 1127–31).

(14) (a) Saveant, J. M.; Vianello, E. *Electrochim. Acta* **1967**, *12*, 1545–1561. (b) Andrieux, C. P.; Nadjo, L.; Saveant, J. M. *J. Electroanal. Chem.* **1970**, *26*, 147–186. (c) Amatore, C.; Saveant, J. M. *Ibid.* **1983**, *144*, 59–67. (d) Saveant, J. M. *Acta Chem. Scand., Ser. B* **1983**, *37*, 365–378.

(15) Saveant, J. M.; Vianello, E. *Electrochim. Acta* **1967**, *12*, 629–646.

(16) The whole kinetic analysis is carried out under the assumption that the electron transfer is a fast process within the range of accessibile sweep rates. This is the case under most experimental conditions for aromatic organic molecules. When necessary, the complication of a slow charge transfer in the kinetic analysis can be dealt with according to previously published procedures.[17]

(17) Nadjo, L.; Saveant, J. M. *J. Electroanal. Chem.* **1973**, *48*, 113–145.

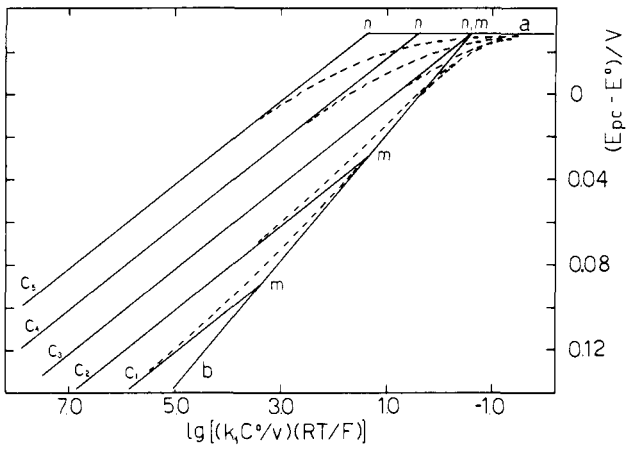

Figure 1. Schematic representation of the DISP1–DISP2 competition under pure kinetic conditions. Variation of the cathodic peak potential with the kinetic parameter $(k_1C^0/v)(RT/F)$. Solid lines correspond to the limiting behavior: (a) diffusion; (b) DISP1; (c) DISP2, with the following value of the parameter k_{-1}/k_2: $C_1 = 10^{-2}$, $C_2 = 10^{-1}$, $C_3 = 1.0$, $C_4 = 10$, $C_5 = 10^2$. Points m correspond to $(k_{-1}k_1^{1/2}/k_2)(RTC^0/Fv)^{1/2} = 0.5$. Points n indicate the passage from pure kinetic to diffusion regimes. Dashed lines represent the actual variation of E_p.

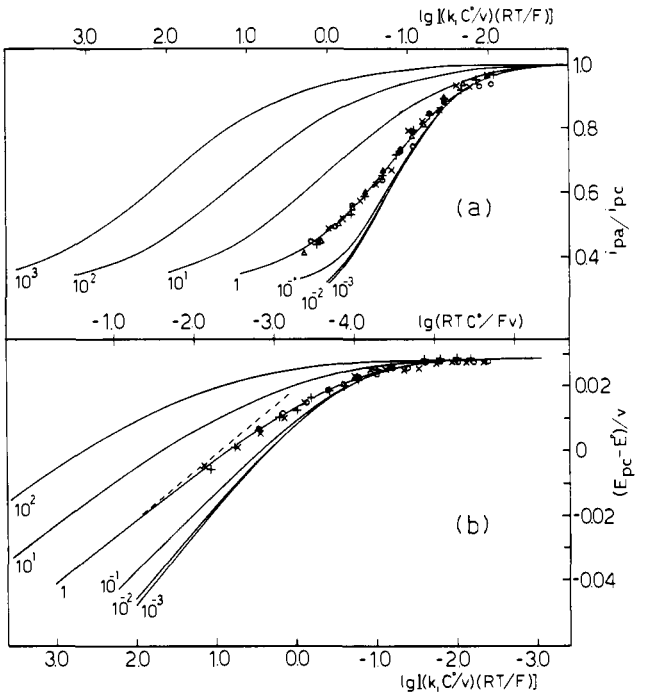

Figure 2. The DISP1–DISP2 competition under mixed kinetic-diffusion control. Working curves relating (a) the anodic to cathodic peak current ratio, i_{pa}/i_{pc}; (b) the cathodic peak potential, E_p, to the kinetic parameter, $(k_1C^0/v)(RT/F)$, for a series of values of the competition parameter, k_{-1}/k_2, as reported on each curve. The points in (a) and (b) represent the experimental values of i_{pa}/i_{pc} and E_p^c, respectively, obtained with phthalimide in dry DMF + 0.1 M NBu_4ClO_4 at 25 °C; C^0 (mM) = 0.5 (○), 0.95 (×), 2.2 (+), 4.95 (△), varying v from 0.008 to 25 V s^{-1}. The central abscissa, is common to (a) and (b) and refers to the variation of the experimental parameters. The upper and lower abscissas indicate the variation of the theoretical parameter relative to the i_{pa}/i_{pc} and E_{pc} curves, respectively.

When the overall rate constant of the chemical process is large within the time scale of the experiment, a stationary state is reached concerning the concentrations of $AH^{-}\cdot$ and AH_2 resulting from mutual compensation of the chemical and diffusion processes. The gradient of these two species are thus confined within a reaction layer adjacent to the electrode surface, the thickness of which is small as compared to the diffusion layer. The wave under investigation is then totally irreversible whatever the sweep rate. Under these conditions the cathodic peak potential is a convenient measure of the kinetics of the overall reaction. Simple expressions[14] (Table I) of the peak potential as a function of the various parameters (rate constants, sweep rate, concentration) are obtained in each case where the kinetic control is by a single rate-determining step. We can distinguish four different limiting behaviors. The ECE regimes correspond to the second electron transfer at the electrode (2) prevailing on the homogeneous transfer of the second electron (2′), while the DISP regimes refer to the opposite situation. Two ECE subcases are further distinguished according to the value of the equilibrium constant of the protonation reaction. If this is in favor of $AH_2\cdot$, we obtain the ECE_{irr} case, whereas the ECE_{rev} case is obtained in the converse situation. Two DISP subcases are also distinguished: DISP1 features the case where the protonation reaction 1 is the rate-determining step, whereas in the case of DISP2, reaction 1 remains at equilibrium, the rate-determing step being now the homogeneous electron transfer 2′. In each of these four limiting situations, the cathodic peak potential is a linear function of log v and log C^0 (v and C^0 are the sweep rate and initial concentration, respectively). An important element of the mechanism analysis, under these conditions, is thus provided by the slopes of the E_p - log v and E_p - log C^0 diagrams. The slopes corresponding to each of the four regimes are listed in Table I. They essentially allow one to distinguish second-order behaviors (DISP2) from first-order behaviors (ECE_{irr}, ECE_{rev}, DISP1).

A given experimental system may well, however, not correspond to such limiting situations where kinetic control is by a single rate-determining step. In most practical situations, it is sufficient to deal with the transitions between two different limiting situations. In addition to the overall rate constant, the kinetics now depend upon an additional parameter, which reflects the competition between the two limiting kinetic regimes. The expressions of these dimensionless competition parameters are given in Table I. Note that variation of the experimentally adjustable parameters (v and C^0) allows shifting the system from one limiting situation to the other. Figure 1 gives an illustration of the passage between two limiting situations, namely, DISP1 and DISP2, which proved to be most useful in the analysis of the experimental data reported below. The transition limit between DISP1 and DISP2 is indicated in this schematic representation by the intersection points m of the limiting straight lines and corresponds to a value of the parameter $(k_1^{1/2}k_{-1}/k_2)(RTC^0/Fv)^{1/2}$ equal to 0.5.

When the overall chemical process involves characteristic times falling within the time scale of the experiment, the "pure kinetic" conditions are no longer fulfilled. The electrochemical reaction is then under the control of both the chemical and the diffusion processes: the concentration profiles of $AH^{-}\cdot$ and AH_2 encompass the whole diffusion layer. The wave is now quasi-reversible in the sense that a partial reversibility can be obtained upon scan reversal. The latter increases as the sweep rate is raised, or the concentration and overall rate constant is decreased until a reversible pattern is observed. The middle point between the anodic and cathodic peak is then located at the standard potential ($E°$) of the $AH/AH^{-}\cdot$ couple. Under these mixed kinetic control conditions, it is still possible to use the cathodic peak potential as a measure of the overall kinetics. Figure 1 shows how the relevant kinetic parameter featuring the regimes DISP1 and DISP2 can be determined from the intersection points n of the straight lines corresponding to limiting behaviors. Similar procedures can be used for any of the other kinetic regimes. However, such determinations of the rate constants are usually not very accurate owing to the error on peak potential measurements (±1 mV) and because it is often difficult to reach experimentally the limiting lines characteristic of the pure kinetic and diffusion conditions. The ratio between the anodic, i_{pa}, and cathodic, i_{pc}, peak current then offers a more accurate access to the rate constant. Table II gives a list of the partial derivative equations to be numerically solved taking into account the appropriate initial and boundary conditions in each of the limiting regimes for obtaining the working curves relating i_{pa}/i_{pc} to the corresponding kinetic parameter. The working curves for DISP1 and DISP2 are shown on Figure 2. In the same figure are also reported the

Table II. Kinetic Analysis of Self-Protonation Mechanisms by Cyclic Voltammetry: Mixed Kinetic-Diffusion Control[a]

kinetic regime	partial derivative equation to be numerically computed
ECE_{irr}	$\partial a/\partial\tau = \partial^2 a/\partial y^2 - \lambda_1 ab\ \partial b/\partial\tau = \partial^2 b/\partial y^2 - \lambda_1 ab\ \partial c/\partial\tau = \partial^2 c/\partial y^2 + \lambda_1 ab$
ECE_{rev}	$\partial a/\partial\tau = a^2/a/\partial y^2 - \lambda_1\{ab - (2/3K)c(1 - a - b - c)\}$ $\partial b/\partial_\tau = a^2 b/\partial y^2 - \lambda_1\{ab - (2/3K)c(1 - a - b - c)\}$ $\partial c/\partial\tau = \partial^2 c/\partial y^2 + \lambda_1\{ab - (2/3K)c(1 - a - b - c)\}$
DISP1	$\partial a/v\tau = \partial^2 a/\partial y^2 - \lambda_1 ab\ \partial b/\partial\tau = \partial^2 b/\partial y^2 - 2\lambda_1 ab$
DISP2	$\partial a/\partial\tau = \partial^2 a/\partial y^2 - (3\lambda_1\lambda_2/2\lambda_{-1})\{ab^2/(1 - a - b)\}\ \partial b/\partial\tau = \partial^2 b/\partial y^2 - (3\lambda_1\lambda_2/\lambda_{-1})\{ab^2/(1 - a - b)\}$
initial and boundary conditions	
$\tau = 0, y > 0; y = \infty, \tau > 0, a = 1, b = c = 0\ y = 0, \tau > 0, a = b \exp(-\xi), c = 0\ \partial a/\partial y = -\partial b/\partial y + \partial c/\partial y = i/FSC^\circ D^{1/2}(Fv/RT)^{1/2}$	

competition parameters			
ECE_{rev}–ECE_{irr}	k_1/k_1	$\rightarrow 0$	ECE_{rev}
		$\rightarrow \infty$	ECE_{irr}
ECE_{irr}–DISP1	k_2/k_1	$\rightarrow 0$	ECE_{irr}
		$\rightarrow \infty$	DISP1
DISP1–DISP2	k_{-1}/k_2	$\rightarrow 0$	DISP1
		$\rightarrow \infty$	DISP2
DISP2–ECE_{rev}	$K_1^{1/2}k_1/k_2$	$\rightarrow 0$	DISP2
		$\rightarrow \infty$	ECE_{rev}

[a] $a = C_{AH}/C^\circ$, $b = C_{AH^{-\cdot}}/C^\circ$, $c = C_{AH_2^{-\cdot}}/C^\circ$, $y = x(Fv/RTD)^{1/2}$, $\tau = Fvt/RT$, $\xi = -F/RT(E - E^\circ)$, t = time, x = distance from the electrode surface, D = diffusion coefficient, C° = initial concentration, v = sweep rate, S = electrode surface area, E° = standard potential of the $AH/AH^{-\cdot}$ couple, $E = E_i - vt$ during the cathodic scan, $E = 2E_f + E_1 + vt$, E_1 = starting potential, E_f = switching potential.

working curves relating $E_p - E^\circ$ to $(k_1C^0/v)(RT/F)$. These curves serve two purposes: fitting of the experimental data both gives access to the reaction mechanism and provides the value of the overall rate constant.

As in the preceding case, a given experiment may well fall out of any limiting situation and involve the competition between two of them. It is therefore useful to give (Table II) the expressions of the competition dimensionless parameter under mixed kinetic-diffusion control. We note that the transition between two limiting situations does not necessarily correspond to the same range of values of the experimental parameters under pure kinetic and mixed kinetic-diffusion controls. For example, the passage between DISP1 and DISP2 corresponds to $(k_{-1}k_1^{1/2}/k_2)(RTC^0/Fv)^{1/2}$ in pure kinetic conditions, and to k_{-1}/k_2 under mixed kinetic-diffusion control. Working curves can also be computed for the transition between two limiting situations by numerical resolution of similar, although somewhat more complicated partial derivative equations, to those listed in Table II. Figure 2 gives a set of working curves obtained for various values of the DISP1–DISP2 competition parameter k_{-1}/k_2. Analysis of the mechanism and rate constant determination then requires a two-parameter fitting of the experimental data.

To help analyze the four-cornered ECE_{irr}–ECE_{rev}–DISP2–DISP1 competition, a schematic zone diagram[2g,19a] is shown in Figure 3 for both pure kinetic and mixed kinetic-diffusion conditions. Each point on the diagram represents a particular kinetic state of the system. The boundary lines are drawn for a unit value of the corresponding competition parameter (Tables I and II). The dashed lines in the central zone underline the fact that, in this region, all steps participate to the kinetic control and thus that the predicted behavior lies inbetween the limiting behavior described in Tables I and II (see ref 19 for an analysis of this problem in the related case of a standard ECE–DISP reaction scheme). The way in which the variation of the experimental

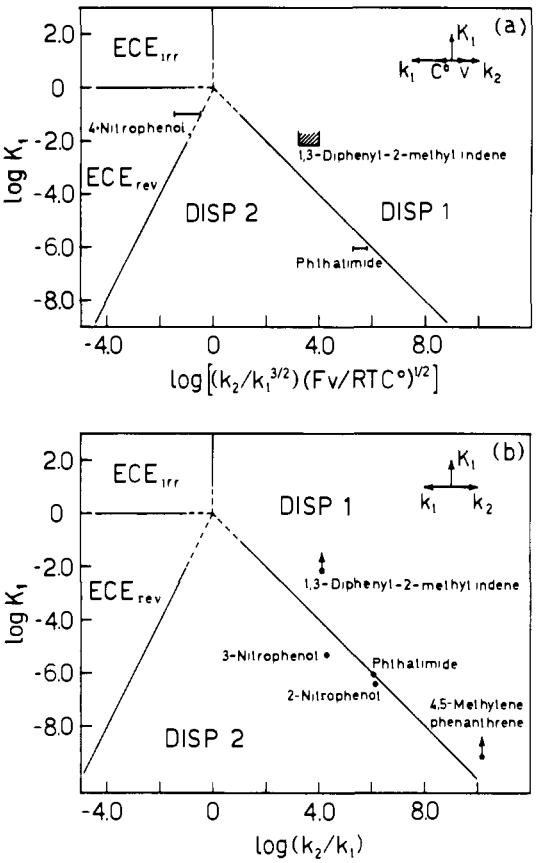

Figure 3. Kinetic zone diagram: (a) pure kinetic conditions, (b) mixed kinetic-diffusion conditions.

parameters shifts the kinetic state of the system is represented by a set of arrows on each diagram.

Phthalimide. The main qualitative characteristics of the reduction of phthalimide have already been described.[8a,b,9a] We recast them briefly for a better understanding of the following quantitative kinetic analysis. Figure 4a shows two typical cyclic voltammograms obtained at 0.1 and 25 V s^{-1}, respectively. The simplest behavior is observed at 25 V s^{-1} where two chemically reversible one-electron waves are recorded.[18] The two successive waves here simply correspond to the stepwise formation of $AH^{-\cdot}$ and AH^{2-}. At low sweep rate the first wave is irreversible corresponding to the transfer of (2/3) electron per molecule while the second is partially reversible and corresponds to the transfer of (4/3) electron per molecule of starting material. In these conditions both A^- and AH_3 are produced, as a consequence of self-protonation taking place according to mechanisms I or II. Both products are simultaneously reduced at the second wave potentials. A^- undergoes a reversible one-electron transfer while AH_3 gives rise to an irreversible two-electron process.[9a] These observations are compatible with the overall formation of $(2/3)A^-$ and $(1/3)AH_3$ upon reduction of the starting AH at the first wave. This is confirmed by controlled potential electrolysis which leads to the passage of (2/3)e per molecule and to the formation of A^- and AH_3 in the expected ratio 2/1. Also, addition of a proton donor to the solution of AH results in an increase of the first wave from (2/3)e to 2e per molecule.

The overall stoichiometry of the first reduction thus matches what is expected for mechanisms I and II, and clearly rules out the hydrogen evolution mechanism. On the other hand, as can be seen in Figure 4, $E^\circ_{AH/AH^{-\cdot}} - E^\circ_{AH^{-\cdot}/AH^{2-}} = 800$ mV, and thus the equilibrium constant for the disproportionation reaction:

$$2AH^{-\cdot} \rightleftarrows AH + AH^{2-}$$

is 3×10^{-14}. The maximal value of the backward reaction rate constant is the diffusion limit, i.e., 5×10^9 M^{-1} s^{-1} in DMF. The forward reaction rate constant is thus at most equal to 1.5×10^{-4} M^{-1} s^{-1} leading to a half-life of about 10^6 s for $AH^{-\cdot}$. This is clearly

(18) While electron transfer appears as fast at the first wave, the second wave exhibits a slow charge-transfer behavior resulting in a lower peak current and a definitely larger potential separation between the anodic and the cathodic peaks.

(19) (a) Amatore, C.; Saveant, J. M. *J. Electroanal. Chem.* **1977**, *85*, 27–46. (b) Amatore, C.; Saveant, J. M. *Ibid.* **1979**, *102*, 21–40.

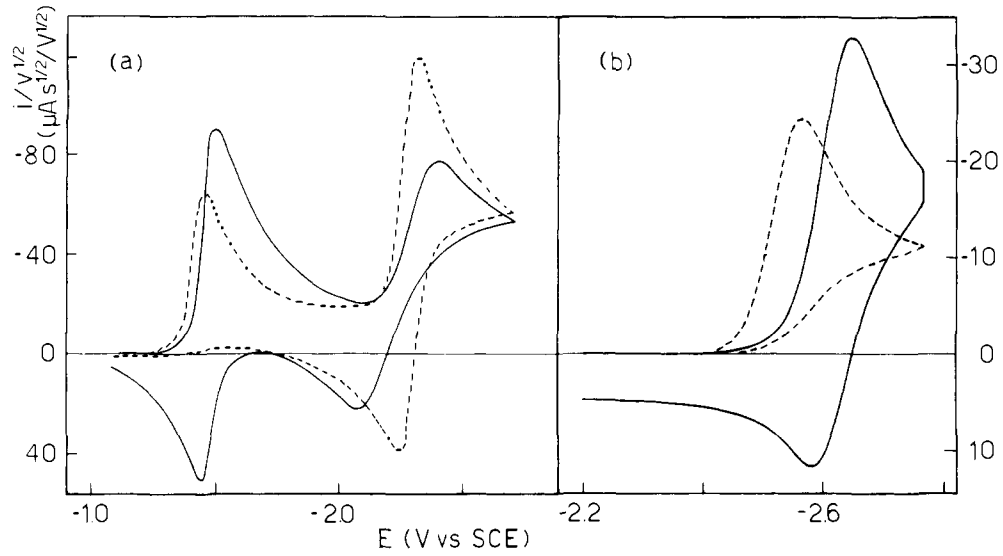

Figure 4. Cyclic voltammograms of (a) phthalimide, (b) 1,3-diphenyl-2-methylindene in dry DMF + NBu_4ClO_4, 0.1 M: (a) 25 °C, C^0 = 5.0 mM, v = 0.1 (---) and 25 (—) V s^{-1}; (b) 20 °C, C^0 = 2.6 mM, v = 0.1 (---) and 150 (—) V s^{-1}.

incompatible with the behavior shown in Figure 4a which indicates that the $AH^{-}\cdot$ half-life is less than 0.25 s, which rules out the occurrence of mechanism II.[21]

A more complete kinetic investigation of the reaction in the context of mechanism I involves the analysis of the E_p – log v and E_p - log C^0 data on one hand and of the i_{pa}/i_{pc} data on the other. These are shown on Figures 2b and 2a, respectively. It is seen that the i_{pa}/i_{pc} data obtained for various values of the sweep rate and concentration fit the working curve featuring a DISP1–DISP2 competitive mechanism for a value of the competition parameter $k_{-1}/k_2 = 1$. The best fit is obtained for $k_1 = 4.2 \times 10^3$ M^{-1} s^{-1}. Analogous fit of the experimental data with the (E_p - $E°$) - log (C^0/v) working curves is shown in Figure 2b. It is seen that a satisfactory fit occurs with the curve calculated for the same competition parameter. The value found for k_1 is now 2×10^3 M^{-1} s^{-1}. The difference with the k_1 value determined from i_{pa}/i_{pc} may be attributed to a lower accuracy of the peak potential determination. It can also be noticed that in our experimental conditions the linear oblique portion of the working curve is hardly reached. This is due to the fact that, being k_1 relatively small, too low v or too high C^0 values would be necessary to achieve pure kinetic conditions, corresponding to the linear portion, with a slope of 19.7 mV/log (C^0/v) unit. The resulting value of the DISP1–DISP2 competition parameter $(k_{-1}k_4^{1/2}/k_2)(C^0RT/Fv^{1/2})$ is 4.0 at v = 0.008 V s^{-1}, while its value at the transition between DISP1 and DISP2 would be 0.5 (see Figure 1). This shows, as predicted in the first section, that within the framework of the DISP1–DISP2 competition the system is closer to the DISP2 situation under pure kinetic conditions than under mixed kinetic diffusion control, in agreement with the observation that the slope of the linear oblique portion of the E_p vs. log (C^0/v) is close to 19.7 (Figure 2b). This can also be seen on the two zone diagrams of Figure 3 where the representative points of the system have been located under the assumption that k_2 and k_{-1} are close to the diffusion limit.[20]

1,3-Diphenyl-2-methylindene. Figure 4b shows two typical cyclic voltammograms obtained at 0.1 and 150 V s^{-1}, respectively. There is only one wave within the available potential range. This becomes increasingly reversible at high sweep rates featuring the formation of the anion radical $AH^{-}\cdot$ which is then stable within the corresponding time scale. At lower sweep rates, the wave becomes irreversible and tends toward a peak height corresponding to

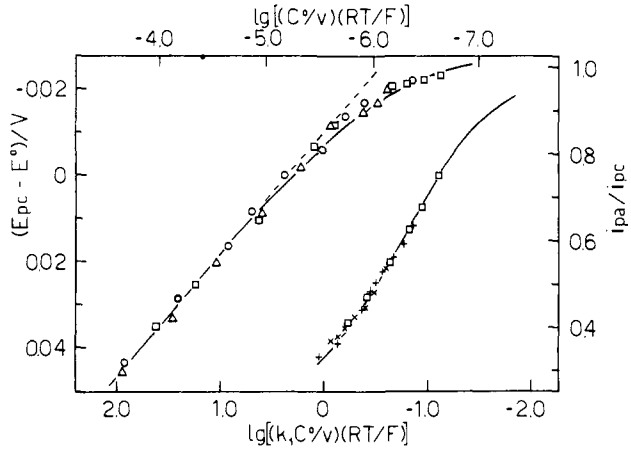

Figure 5. Reduction of 1,3-diphenyl-2-methylindene in dry DMF + NBu_4ClO_4 0.1 M at 20 °C. Variation of the cathodic peak potential (left curve) and of the ratio of anodic to cathodic peak current ratio (right curve) with the experimental parameters reported on the upper abscissa: C^0 (mM) = 1.4 (□), 2.6 (+), 2.8 (○), 6.1 (×), 9.0 (△). The sweep rate was varied between 0.1 and 200 V s^{-1}. The solid lines (lower abscissa scale) are the working curve obtained for $k_{-1}/k_2 = 10^{-2}$ and $k_1 = 3.5 \times 10^5$ M^{-1} s^{-1}.

(2/3)e per molecule. Addition of phenol converts the wave into a two-electron peak. Preparative-scale electrolysis yields (1/3) A^- corresponding to the passage of (2/3) e per molecule. These main qualitative characteristics of the reduction of 1,3-diphenyl-2-methylindene have previously been described.[9e] They are again compatible with mechanisms I and II and clearly rule out the occurrence of the hydrogen evolution mechanism. Since there is no second wave we have no data giving $E°_{AH^{-}\cdot/AH^{2-}}$. However, this is certainly more negative than the discharge of the supporting electrolyte. It follows that $E°_{AH/AH^{-}\cdot} - E°_{AH^{-}\cdot/AH^{2-}}$ > 300 mV, and thus the disproportionation equilibrium constant is less than 10^{-5}. The disproportionation rate constant is thus at most 5×10^4 M^{-1} s^{-1}, probably much less, which corresponds to a half-life larger than 7 ms which is not compatible with the experiments reported in Figure 4b in which it is seen that the chemical reversibility is hardly reached at 150 V s^{-1} (equivalent to a half-life of 0.2 ms). This rules out the possible occurrence of mechanism II. The E_p - log v, E_p - log C^0, and i_{pa}/i_{pc} data shown in Figure 5 should thus be analyzed in the framework of the only remaining possible mechanism, i.e., mechanism I. The linear oblique portion of the E_p variation exhibits a slope of 29 mV. This is in agreement with a DISP1 situation, for which a slope of 29.1 mV is foreseen at 20 °C. This is confirmed by the i_{pa}/i_{pc} data.

(20) The diffusion limit can be estimated as equal to 5×10^9 and 2×10^9 M^{-1} s^{-1} in DMF and Me_2SO, respectively:[20b] Kojima, H.; Bard, A. J. *J. Am. Chem. Soc.* **1975**, *97*, 6317–6324.

(21) In the case where the forward disproportionation reaction is not the rate-determining step, i.e., if the latter is the protonation of AH^{2-} by AH, the overall rate constant is lower than the forward disproportionation rate constant.

It is indeed seen that $k_{-1}/k_2 \leq 10^{-2}$, the value obtained for k_1 being a 3.5×10^5 M^{-1} s^{-1}.

Assuming that k_2 is close to the diffusion limit,[20] the system is represented in the two zone diagrams as shown in Figure 3. Although the exact location of the representative points is not known it is seen that they unambiguously belong to the DISP1 zone.

4,5-Methylenephenanthrene. The self-protonation reaction is dramatically slower with the title compound than with phthalimide and 1,3-diphenyl-2-methylindene. The reaction is actually so slow that conventional techniques of homogeneous kinetics can be used to follow the decay of the anion radical $AH^{-}\cdot$ in the presence of various amounts of the starting material.

Cyclic voltammetry exhibits a single reversible one-electron wave. Upon addition of phenol it is converted into an irreversible two-electron peak featuring the 2e + $2H^+$ reduction of AH into AH_3. Preparative-scale electrolysis carried out in the latter conditions gives rise to the passage of 2e per molecule. The product recovered upon workup has been identified by its NMR spectrum as 9,10-dihydro-4,5-methylenephenanthrene (AH_3). It exhibits a multiplet at 7.1 ppm corresponding to six aromatic hydrogen atoms, a singlet at 3.8 ppm, and another at 303 ppm ascribed to two and four hydrogen atoms, respectively, in agreement with a 3:1:2 integration ratio.

Electrolyses carried out in the absence of exogeneous proton donors give rise to the transfer of 0.7 (2/3) e per molecule and shows an anodic wave at much more positive potentials, which can be assigned to the oxidation of A^-. The addition of a proton donor to the electrolyzed solution results in the disappearance of this wave and the partial regeneration of the cathodic peak of the substrate. The solid recovered upon workup is a mixture of two products. The NMR spectrum recorded after acidification shows the characteristic lines of both the starting materials and two-electron reduction product, AH_3. The ratio of the two methylenic protons of each compound indicates that the AH/AH_3 ratio is 2.

The anion radical was produced by preparative scale electrolysis and its decay with time measured from the height of its oxidation wave. This was done at various concentrations of the starting material, all in excess with respect to the $AH^{-}\cdot$ concentration, so as to ensure pseudo-order conditions. The kinetics was thus found to be first order toward $AH^{-}\cdot$. The pseudo-first-order apparent rate constant was then plotted vs. the concentration of AH (Figure 6). It is observed that the resulting straight line does not go through the origin. This can be rationalized in terms of a parallel decay of the anion radical not due to the reaction with AH. Several possibilities exist in this connection. $AH^{-}\cdot$ may decompose spontaneously giving rise to A^- and hydrogen evolution similarly to what has been previously hypothesized with substituted fluorenes and other compounds.[13] It may also abstract protons from the remaining proton donors, i.e., trace water, the quaternary ammonium cation of the supporting electrolyte, the solvent itself, and the reduction product, AH_3, present as a result of the preparative electrolysis. In connection with the latter point, it was noticed that addition of AH_3 to the reaction mixture slightly increases the apparent rate constant.

The overall homogeneous kinetics of the self-protonation reaction is expressed as:

$$dC_{AH^{-}\cdot}/dt = (2k_1k_2/k_{-1})C_{AH}C_{AH^{-}\cdot}^{2}/[C_{A^-} + (k_2/k_{-1})C_{AH^{-}\cdot}]$$

leading to two limiting behaviors as a function of k_2/k_{-1}. When $k_2C_{AH^{-}\cdot} << k_{-1}C_{A^-}$:

$$-dC_{AH^{-}\cdot}/dt = (2k_1k_2/k_{-1})C_{AH}C_{AH^{-}\cdot}/C_{A^-}$$

which corresponds to the DISP2 situation. When $k_2C_{AH^{-}\cdot} >> k_{-1}C_{A^-}$:

$$-dC_{AH^{-}\cdot}/dt = 2k_1C_{AH}C_{AH^{-}\cdot}$$

which corresponds to the DISP1 situation.

The experimental data (Figure 6) indicate that the DISP1 kinetics are followed, i.e., that $k_2 > k_{-1}$. It is then found that $k_1 = 0.37$ M^{-1} s^{-1}.

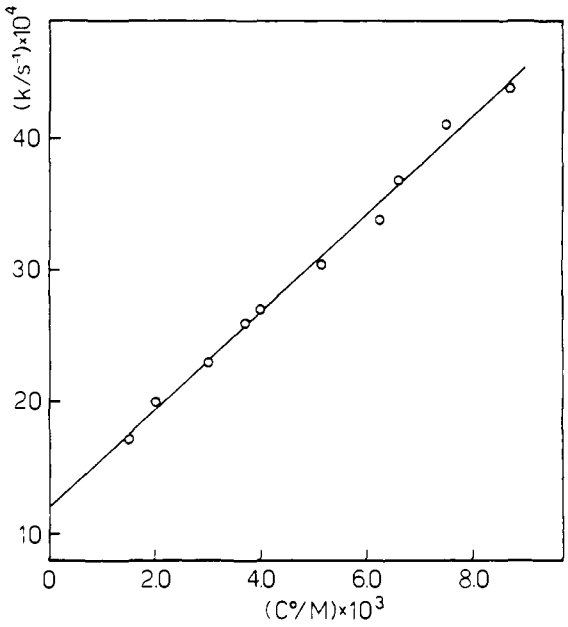

Figure 6. Self-protonation in the reduction of 4,5-methylenephenanthrene. Variation of the apparent pseudo-first-order rate constant with the concentration of starting material in dry DMF + NBu_4ClO_4, 0.1 M at 16 °C.

Nitrophenols. The electron and proton stoichiometries are now different from the preceding cases. By preparative scale electrolysis in Me_2SO the 6e hydroxyphenylamino derivative is obtained in the case of the 2 and 4 isomers, together with the conjugate base of the starting material, $^{-}OC_6H_4NO_2$, in a ratio of 1/6.[9d] With the 3 isomer the reduction yields the 4e product hydroxyphenylhydroxylamine and the conjugate base, $^{-}OC_6H_4NO_2$, in a ratio of 1/4.[9c] The apparent coulometric n values are 0.85 and 0.80 e per molecule, respectively. This corresponds, for the 3 isomer, to the overall stoichiometry:

$$HOC_6H_4NO_2 + (4/5)e \rightarrow (4/5)^{-}OC_6H_4NO_2 + (1/5)HOC_6H_4NHOH + (1/5)H_2O$$

The reaction sequence matching this stoichiometry has been shown to involve the following initial steps:[9c]

$$HOC_6H_4NO_2 + e \rightleftarrows HOC_6H_4NO_2^{-}\cdot$$

$$HOC_6H_4NO_2^{-}\cdot + HOC_6H_4NO_2 \underset{k_{-1}}{\overset{k_1}{\rightleftarrows}} HOC_6H_4NO_2H\cdot + {}^{-}OC_6H_4NO_2$$

$$HOC_6H_4NO_2H\cdot + HOC_6H_4NO_2^{-}\cdot \xrightarrow{k_2} HOC_6H_4NO_2H^{-} + HOC_6H_4NO_2$$

$$HOC_6H_4NO_2H^{-} + HOC_6H_4NO_2 \rightarrow HOC_6H_4NO + {}^{-}OC_6H_4NO_2 + H_2O$$

p-Nitrosophenol, which is more easily reducible than the parent compound by ca. 300 mV,[9c] undergoes a fast decay, involving the following electron and proton transfer reactions:

$$HOC_6H_4NO + HOC_6H_4NO_2^{-}\cdot \rightarrow HOC_6H_4NO^{-}\cdot + HOC_6H_4NO_2$$

$$HOC_6H_4NO^{-}\cdot + HOC_6H_4NO_2 \rightarrow HOC_6H_4NOH\cdot + {}^{-}OC_6H_4NO_2$$

$$HOC_6H_4NOH\cdot + HOC_6H_4NO_2^{-}\cdot \rightarrow HOC_6H_4NOH^{-} + HOC_6H_4NO_2$$

$$HOC_6H_4NOH^{-} + HOC_6H_4NO_2 \rightarrow HOC_6H_4NHOH + {}^{-}OC_6H_4NO_2$$

This corresponds to the usual reaction scheme describing the reduction of aromatic nitro derivatives in dipolar aprotic solvents,

Table III. Redox and Self-Protonation Constants

compound	phthalimide[a]	1,3-diphenyl-2-methylindene[a]	4,5-methylene-phenanthrene[a]	2-nitrophenol[b]	3-nitrophenol[b]	4-nitrophenol[b]
$E^\circ_{AH/AH^{-\cdot}}$ (V vs. SCE)	−1.47	−2.62	−2.32	−0.87	−1.10	−1.26
k_1 (M^{-1} s^{-1})	4.2×10^3	3.5×10^5	0.37	7.2×10^2	1×10^4	$\lesssim 2 \times 10^7$ [d]
k_{-1}/k_2	1.0	$\leq 10^{-2}$	≤0.1	1.66	10	> 2
$pK_{AH/A^{-\cdot}}$ [c,25]				7.2	8.4	7.1
$pK_{AH_2^{+\cdot}/AH^{-\cdot}}$ [c,26]				2.0	3.1	3.6

[a] In DMF. [b] In Me_2SO. [c] In water. [d] Rough estimation (see text).

with the only difference that in our case the parent compound provides the necessary protons instead of an exogenic proton donor.[22]

For the 2 and 4 isomers dehydration of hydroxyphenylhydroxylamine to the corresponding quinone imine, followed by electron and proton transfers, yielding finally the 2- and 4-hydroxyanilines, must be taken into account:[9d]

$$HOC_6H_4NHOH \rightarrow OC_6H_4NH + H_2O$$

$$OC_6H_4NH + HOC_6H_4NO_2^{-\cdot} \rightarrow OC_6H_4NH^{-\cdot} + HOC_6H_4NO_2$$

$$OC_6H_4NH^{-\cdot} + HOC_6H_4NO_2 \rightarrow OC_6H_4NH_2^{\cdot} + {}^-OC_6H_4NO_2$$

$$OC_6H_4NH_2^{\cdot} + HOC_6H_4NO_2^{-\cdot} \rightarrow {}^-OC_6H_4NH_2 + HOC_6H_4NO_2$$

$${}^-OC_6H_4NH_2 + HOC_6H_4NO_2 \rightarrow HOC_6H_4NH_2 + {}^-OC_6H_4NO_2$$

This leads to the following overall stoichiometry for the 2 and 4 isomers:

$$HOC_6H_4NO_2 + (6/7)e \rightarrow (6/7){}^-OC_6H_4NO_2 + (1/7)HOC_6H_4NH_2 + (2/7)H_2O$$

This reaction sequence, which matches the conditions of preparative electrolysis for both the 2 and the 4 isomers, holds in the voltammetric time scale only for the 4 isomer. With 2-nitrophenol, in fact, an anodic peak is observed in cyclic voltammetry, which can be assigned to the oxidation of 2-hydroxyphenylhydroxylamine, presumably due to its slow dehydration to benzoquinonimine. Consequently 2-nitrophenol can be considered to involve the same stoichiometry as the 3 isomer in the voltammetric time scale.

In the above reaction schemes the electron-transfer steps following the protonation of the initial anion radical have been depicted as homogeneous reactions. This is strictly true in the case where the protonation of the anion radical is not too fast so that the various rediculble species resulting from its protonation are formed at a large distance from the electrode and are reduced homogeneously, by the anion radical, before having time to diffuse back to the electrode and be reduced at its surface. In other words this description fits with a DISP regime. For faster protonation reactions, reduction at the electrode surface in the framework of an ECE reaction scheme will prevail. In all cases the kinetics of the system is the same as with the two-electron systems described above. The only changes concern the stoichiometric coefficients.

For the three nitrophenol isomers the rate constant of the disproportionation reaction

$$2HOC_6H_4NO_2^{-\cdot} \rightleftarrows HOC_6H_4NO_2 + HOC_6NO_2^{2-}$$

as obtained using the same procedure as for the other compounds is much too low to be compatible with the observed half-lives of the anion radicals, again ruling out mechanism II.

2-Nitrophenol. The first reduction peak of 2-nitrophenol is chemically irreversible at low sweep rates, owing to the self-protonation reaction sequence following the first-electrode uptake. However, full reversibility is reached increasing the sweep rate, and $i_{pa}/i_{pc} \simeq 1$ at 40 V s^{-1}. The variations of E_{pc} and i_{pa}/i_{pc} with

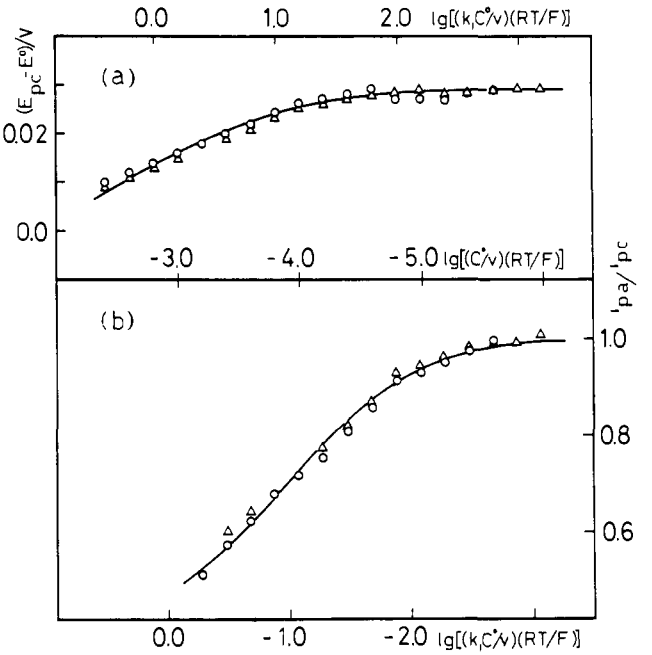

Figure 7. Reduction of 2-nitrophenol in dry Me_2SO + NBu_4ClO_4, 0.1 M at 25 °C. Variation of (a) peak potential and (b) anodic to cathodic peak current ratio with the experimental parameters (central abscissa): C^0 (mM) = 0.94 (△) and 5.0 (○). The sweep rate was varied between 0.006 and 50 V s^{-1}. The solid lines represent the working curves calculated for $k_{-1}/k_2 = 1.66$. The corresponding theoretical parameters are reported in the upper and lower abscissas.

the experimental parameters are reported in Figure 7a and b, respectively. The working curves to be fitted with these data are calculated by computation of differential equations slightly different from those reported in Table II; they include different stoichiometric factors since the initial anion radical, $HOC_6H_4NO_2^{-\cdot}$, is now involved in three successive electron-transfer steps and the parent compound $HOC_6H_4NO_2$ in four successive protonation steps, instead of one and two, respectively, as in the preceding systems. The appropriate differential equations for the DISP1 and DISP2 regimes can be easily derived from those reported in the third and fourth entries of Table I simply by substituting the stoichiometric factors 2 with 4 and 3 with 5. The best fit is obtained for $k_{-1}/k_2 = 1.66$; the value of k_1 derived from i_{pa}/i_{pc} is 8.3×10^2 M^{-1} s^{-1} while a slightly lower value (6.2×10^2 M^{-1} s^{-1}) is obtained from E_p data. The value of the competition parameter k_{-1}/k_2, close to unity, indicates that the system is under mixed DISP1–DISP2 regime.

The slope of the E_p–log C^0/v diagram is about 15 mV at the lowest available sweep rates, which denotes that a pure kinetic regime is never reached in our conditions. However, the theoretical data indicate that an increase of log C^0/v would lead the systems toward a DISP2 regime, characterized by a slope of 19.7 mV, since the DISP2 situation is favored at the expense of DISP1 when passing from a mixed diffusion-kinetic control to pure kinetic conditions, as already observed in the case of phthalimide.

The representative point of the system is shown in Figure 3b. Its location has been determined under the assumption that k_{-1} is at the diffusion limit since k_2 is likely to be close to such a value. The ensuing value of log K_1 is −6.4, i.e., somewhat larger than the value in water that can be derived from previous measurements

(22) Mann, C. K.; Barnes, K. K. "Electrochemical Reactions in Nonaqueous Systems"; Marcel Dekker: New York, 1973; kpp 347–379.

of pK_{AH/A^-} and $pK_{AH_2^{\cdot}/AA^{-\cdot}}$. (Table III). This falls in line with the fact that in the equilibrium solvation factors are expected to

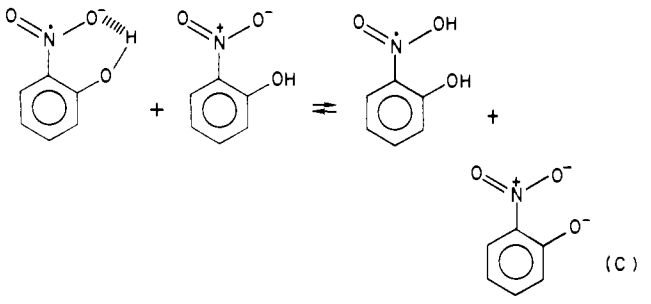

(C)

strongly influence only the stability of the conjugate base of 2-nitrophenol. The other negatively charged species, i.e., the primary anion radical, is likely to be protected against large changes in solvation by internal hydrogen bonding. It follows that K_1 is predicted to be larger in water than in a poor anion solvating solvent such as Me_2SO, in agreement with what was inferred from the above kinetic study.

3-Nitrophenol. Also in this case full reversibility of the first reduction peak can be reached, at a sweep rate of 75 V s^{-1} for $C^0 = 10^{-3}$ M. i_{pa}/i_{pc} data are reported in Figure 8. The best fit is obtained with the working curve corresponding to a value of the DISP1–DISP2 competition parameter $k_{-1}/k_2 = 10$, indicating that the system is practically under DISP2 control. The corresponding value of k_1 is 1×10^4 M^{-1} s^{-1}. The anodic peak is always present, showing that a pure kinetic regime is never reached in the explorable range of C^0 and v values.

The point representing the system in the zone diagram (Figure 3b) was located again assuming that k_{-1} is close to the diffusion limit[20] which would correspond to $k_2 = 2 \times 10^8$ M^{-1} s^{-1}. This results in log $K_1 = -5.3$, i.e., coincident with the value in water (Table III). This is not surprising in view of the fact that in the equilibrium D, the negative charge is likely to be similarly con-

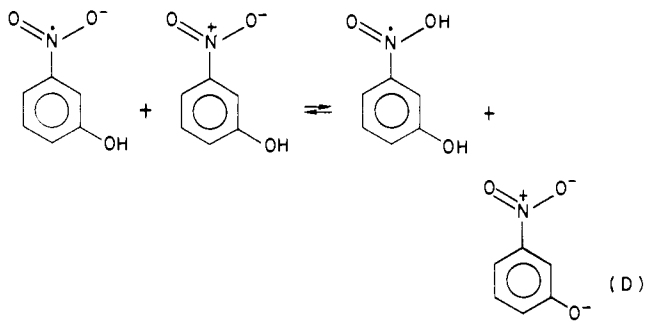

(D)

centrated in the two negatively charged species, i.e., on the NO_2 oxygen of the anion radical and on the phenolic oxygen of the conjugate base. Changes of the solvation free energy of the former are thus expected to be compensated by those of the latter, resulting in the same value of the equilibrium constant.

4-Nitrophenol. Chemical reversibility on the first reduction peak is never reached in the whole range of sweep rate explored, i.e., up to 500 V s^{-1} at 25 °C. This points to a rapid self-protonation reaction. The only source of kinetic and mechanistic information is thus the variation of the cathodic peak potential with v and C^0. The corresponding diagram is shown in Figure 9. The E_p – log (C^0/v) slope is close to 29.6 mV, in the largest part of the explored v and C^0 range.

Above 10 V s^{-1}, E_p becomes independent of concentration, and the E_p/log v slope takes larger values, up to 57 mV at $v \geq 150$ V s^{-1}. It is also noticed that the peak width is about 75 mV in the 29.6-mV slope region and 85 mV in the 57-mV slope region.

In order to obtain further information on the kinetics of the self-protonation reaction, we set out to estimate the standard potential of $AH/AH^{-\cdot}$. Voltammetry was performed at −30 °C, to slow down self-protonation. Measurements were carried out in DMF since use of Me_2SO is prevented at low temperatures. In these conditions an anodic peak can be observed starting from

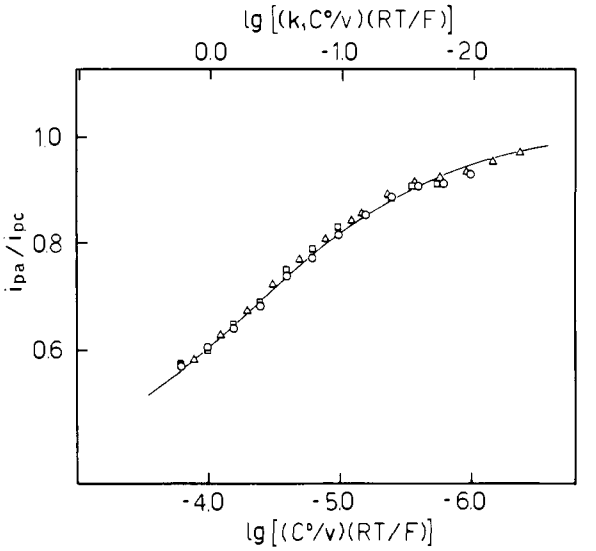

Figure 8. Reduction of 3-nitrophenol in dry Me_2SO + NBu_4ClO_4, 0.1 M at 25 °C. Variation of the anodic to cathodic peak current ratio with the experimental parameters (lower abscissa scale) for C^0 (mM) = 0.55 (□), 0.95 (△), 3.0 (○). The sweep rate was varied between 0.09 and 75 V s^{-1}. The solid line (upper abscissa scale) is the working curve calculated for $k_{-1}/k_2 = 10$.

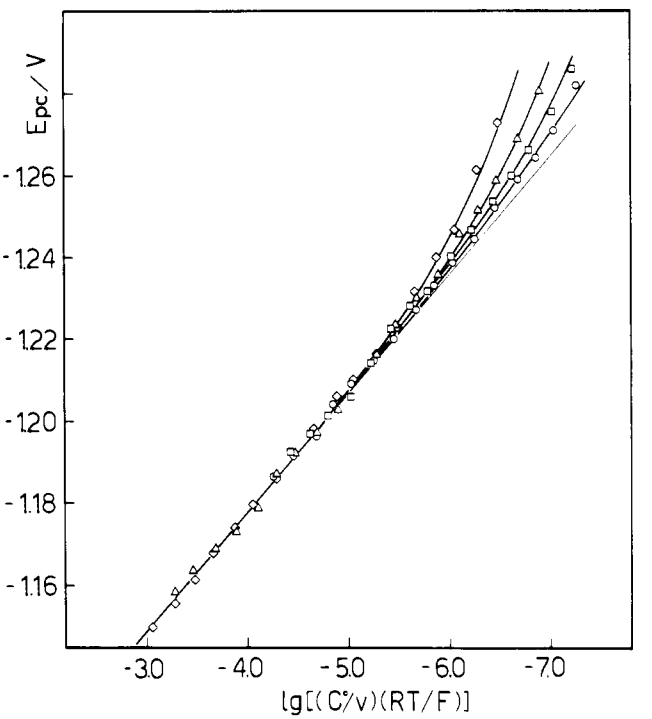

Figure 9. Reduction of 4-nitrophenol in dry Me_2SO + NBu_4ClO_4 0.1 M at 25 °C. Variation of the cathodic peak potential with the experimental parameters for C^0 (mM) = 0.55 (○), 0.94 (□), 2.02 (△), 5.12 (◇). The sweep rate was varied between 0.1 and 400 V s^{-1}.

$v = 4$ V s^{-1}. However, the peak separation $\Delta E_p = E_{pa} - E_{pc}$ is much higher than that expected for a reversible charge transfer. In fact, ΔE_p ranges from 140 mV at $v = 4$ V s^{-1} to 270 mV at $v = 150$ V s^{-1}. The value of $E°$, in these conditions, can be assumed to correspond to $(E_{pa} + E_{pc})/2$. The temperature coefficient of the standard potential has been estimated assuming for it the value for the analogous compounds 4-nitrotoluene and 4-nitroanisole, which was equal to −5 mV in the range −30–25 °C. The solvent effect has been evaluated by measuring the standard potential variation for the same two nitro derivatives, when passing from DMF to Me_2SO at 25 °C. The variation for both was +51 mV, and the same value is assumed also for 4-nitrophenol. With these corrections $E° = -1.26$ V.

A first remark concerns the kinetics of the initial electron-transfer step as can be derived from the E_p–log v data obtained at $v > 150$ V s^{-1} and from the estimated value of the standard potential.[17,23] Taking for the transfer coefficient α a value of 0.55 as an average of that based on the E_p–log v slope ($\alpha = 0.52$) and that obtained from the peak width ($\alpha = 0.57$) and for the diffusion coefficient the value 4.8×10^{-6} cm^2 s^{-1} obtained for 4-nitroanisole in Me_2SO, the apparent charge-transfer standard rate constant is found to be 0.34 cm s^{-1}.

The observation that, at the lower edge of the sweep rate range, E_p varies by ~29.6 mV per decade of C^0/v and that the peak width is 75 mV points to a kinetic control of the ECE_{rev} type. A clear-cut analysis of the problem is not possible since the system appears to fall into an intermediate kinetic situation possibly involving some participation of the four types of kinetic regime. The experimental data seem, however, best accomodated by a kinetic situation close to the ECE_{rev} case for values of log (RTC^0/Fv) ranging from −3 to −5 (above the latter value slow charge transfer may begin to affect E_p[17]). An approximate treatment of the problem then consists in assuming that we are dealing with an ECE_{rev} case[24] with a value of K_1 of about 0.1. Taking into account that the coefficient of the second entry of Table I varies from −0.61 to +0.52 changing from a 2e + 2H$^+$ to a 6e + 6H$^+$ stoichiometry, the resulting value of k_1K_1 is 2×10^6 M^{-1} s^{-1}, i.e., $k_1 = 2 \times 10^7$ M^{-1} s^{-1} and $k_{-1} = 2 \times 10^8$ M^{-1} s^{-1}. The fact that no DISP2 behavior could be detected up to log (RTC^0/Fv) = −5 implies that $k_2 < 10^8$ M^{-1} s^{-1}. The corresponding representative points are shown in Figure 3a.

The values thus derived, although not precise, do not appear unreasonable in view of the following remark. The value of 0.1 for K_1 in Me_2SO is significantly larger than the value which can be estimated for water, 3×10^{-4} (Table III). This falls in line with the fact that in equilibrium E the negative charge is more

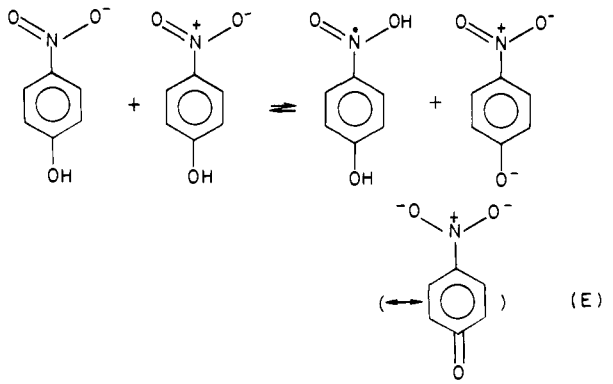

(E)

concentrated in the anion radical (on a nitro oxygen) than in the conjugate base of 4-nitrophenol owing to electron donation by OH in the first case and to delocalization between the nitro and phenoxy groups in the second.

Concluding Remarks

The kinetic investigation described above has shown that, for all six compounds considered in this study, the mechanism of the self-protonation process involves the protonation of the radical anion resulting from the first electron uptake by the starting molecule. This is followed by a homogeneous electron transfer leading to the AH_2^- anion which also reacts on the starting molecule.

The redox and self-protonation constants of the six compounds investigated are summarized in Table III. It is seen that the above-described mechanism is followed within a considerable range of protonation rate constants, covering about eight orders of magnitude.

The first protonation reaction is not always the rate-determing step. It may compete with the next electron-transfer step in this respect. The ratio of the two rate constants, k_{-1}/k_2, of the backward protonation over the forward electron transfer, appears not to take extreme values in at least three cases over six, suggesting that both reactions are probably not too far from the diffusion limit.

This general behavior is illustrated in Figure 3 which summarizes the location of the point representing the system in the kinetic zone diagram. Even in the case of 4-nitrophenol where an ECE_{rev} behavior was observed, the same remark holds.

The case of 4,5-methylenephenanthrene is worth a particular comment in view of the very low value of the self-protonation rate constant. The acidity of the AH /A$^-$ couple is of the same nature as in 1,3-diphenyl-2-methylindene, i.e., benzylic stabilization of the anion. However, the basicity of the AH$^-$· anion radical should be very low in view of the delocalization of the unpaired electron on a three-fused benzene ring system.

Experimental Section

Electrochemical Instrumentation and Procedures. The experiments were carried out in DMF or Me_2SO with 0.1 M Bu_4NClO_4 as supporting electrolyte at 25 °C, except in the case of 1,3-diphenyl-2-methylindene (20 °C) and 4,5-methylenephenanthrene (16 °C).

Potential sweep and cyclic voltammetry were performed with an Eg&G Princeton Applied Research electrochemical instrument formed by a 173 potentiostat equipped with a 179 digital coulometer, a 175 function generator, and a 4203 signal averager. The latter allowed a digital sampling of the voltammetric curves and the determination of the peak potential with an accuracy of about ±1 mV after accumulation and averaging of at least 10 curves. Amperometric curves were recorded with an AMEL Model 448/A apparatus. The working electrode used in the voltammetric experiments was a Pt sphere electrolytically covered by a thin layer of silver and then dipped into mercury. Kinetic amperometric measurements for 4,5-dimethylenephenanthrene were carried out by means of a Pt microelectrode with periodical renewal of the diffusion layer.[27]

The reference electrode was a nonaqueous silver–silver chloride electrode[28a] whose potential was always measured vs. aqueous SCE; all the potentials are given vs. this latter reference electrode. Controlled potential electrolysis and coulometry was performed on a Pt gauze or a Hg pool as working electrode. The procedure for product identification for all the compounds investigated has already been reported,[9a,c-e] with the exception of 4,5-methylenephenanthrene. The two-electron reduction product of the latter has been obtained by controlled potential electrolysis in the presence of phenol and identified by its ^{1}H NMR spectrum, as reported above. ^{1}H NMR analysis was performed on a Varian EM360 spectrometer operating at 60 MHz.

Chemicals. DMF and Me_2SO (C. Erba) were vacuum distilled and stored over neutral alumina (Merck, activity grade I) activated by heating at 400 °C under vacuum for 24 h. NBu_4ClO_4 was prepared from NBu_4OH and $HClO_4$, as previously reported.[28b]

1,3-Diphenyl-2-methylindene was prepared according to the method of Miller and Pittman;[29] all other investigated compounds were reagent grade chemicals, purified by crystallization when necessary.

Acknowledgment. We acknowledge support of this work by the CNRS (Equipede Recherche Associée 309 "Electrochimie Moléculaire") on the French side and by the CNR and the Ministry of Public Education on the Italian side.

Registry No. Phthalimide, 85-41-6; 1,3-diphenyl-2-methylindene, 51310-26-0; 4,5-methylenephenanthrene, 203-64-5; 2-nitrophenol, 88-75-5; 3-nitrophenol, 554-84-7; 4-nitrophenol, 100-02-7.

(23) Matsuda, H.; Ayabe, Y. *Z. Elektrochem.* **1955**, *59*, 494–503.
(24) (a) In a previous investigation of the ECE_{irr}-DISP1 competition in aromatic compounds,[24b] it has been predicted that the DISP1 situation will prevail over the ECE_{irr} situation whenever they can be distinguished, i.e., whenever some chemical reversibility can be observed. The present conclusion does not alter this prediction since on one hand we are dealing here with an ECE_{rev} situation and no chemical reversibility could be observed on the other hand. (b) Amatore, C.; Saveant, J. M. *J. Electroanal. Chem.* **1978**, *86*, 227–232.
(25) Kortüm, G.; Vogel, W.; Andrussow, K. "Dissociation Constants of Organic Acids in Aqueous Solution"; Butterworths: London, 1961.
(26) Hayon, E.; Simic, M. *Acc. Chem. Res.* **1974**, *7*, 114–121.
(27) Farnia, G.; Roffia, S. *J. Electroanal. Chem.* **1981**, *122*, 347–352.
(28) (a) Farnia, G.; Maran, F.; Sandonā, G.; Severin, M. G. *J. Chem. Soc., Perkin Trans. 2* **1982**, *1153*–1158. (b) Capobianco, G.; Farnia, G.; Gambaro, A.; Severin, M. G. *Ibid.* **1980**, 1277–1281.
(29) Miller, W. G.; Pittman, C. U. *J. Org. Chem.* **1974**, *39*, 1955–56.